Metal Doping Regulates Electrocatalysts Restructuring during Oxygen Evolution Reaction

Maoyu Wang[1,2,†], Brian A. Muhich[1,†], Zizhou He[3], Zhenzhen Yang[4], Dongqi Yang[1], Marcos Lucero[1], Hoan Kim Khai Nguyen[1], George E. Sterbinsky[2], Líney Árnadóttir[1], Hua Zhou[2], Ling Fei[3,], Zhenxing Feng[1,*]*

(† These authors contributed equally.)

[1] School of Chemical, Biological and Environmental Engineering, Oregon State University, Corvallis, OR 97331, United States

[2] X-ray Science Division, Argonne National Laboratory, Lemont, IL, 60439, United States

[3] Chemical Engineering Department, University of Louisiana at Lafayette, Lafayette, LA 70504, United States

[4] Chemical Sciences and Engineering Division, Argonne National Laboratory, Lemont, IL, 60439, United States

E-mail: zhenxing.feng@oregonstate.edu, ling.fei@louisiana.edu

Keywords: (Electrocatalyst, Restructuring, Nanocluster, X-ray absorption Spectroscopy, X-ray Photoelectron Spectroscopy)

(High-efficiency and low-cost catalysts for oxygen evolution reaction (OER) are critical for electrochemical water splitting to generate hydrogen, which is a clean fuel for sustainable energy conversion and storage. Among the emerging OER catalysts, transition metal dichalcogenides have exhibited superior activity compared to commercial standards such as RuO_2, but inferior stability due to uncontrolled restructuring with OER. In this study, we create bimetallic sulfide catalysts by adapting the atomic ratio of Ni and Co in $Co_xNi_{1-x}S_y$ electrocatalysts to investigate the intricate restructuring processes. Surface-sensitive X-ray photoelectron spectroscopy and bulk-sensitive X-ray absorption spectroscopy confirmed the favorable restructuring of transition metal sulfide material following OER processes. Our results indicate that a small amount of Ni substitution can reshape the Co local electronic structure, which regulates the restructuring process to optimize the balance between OER activity and stability. This work represents a significant advancement in the development of

efficient and noble metal-free OER electrocatalysts through a doping-regulated restructuring approach.)

1. Introduction

Water splitting reactions to produce hydrogen represent a promising future avenue for clean energy storage and fuels.[1-4] The development of inexpensive and commercially friendly electrocatalysts is essential for the widespread utilization of such processes.[5-7] However, OER remains the key hurdle for the water splitting process, primarily due to sluggish kinetics and large activation energy barriers.[8-11] Enhancing the efficiency of this half-reaction is crucial for achieving the most significant overall energy efficiency gains in energy conversion.[12-14] Currently, noble metal oxides such as RuO_2 and IrO_2 serve as the primary commercial standards for OER electrocatalyst materials. However, their high cost and limited availability hinder their widespread usability.[2, 12, 13, 15] Therefore, it is imperative to develop electrocatalysts based on more earth-abundant 3d transition metal materials.

One essential aspect of discussion regarding all forms of electrocatalysts is their stability under operating conditions. While current standard catalysts such as IrO_2 and RuO_2 exhibited reasonably high chemical stability in both acidic and alkaline media, transition metal catalysts used in OER reactions generally suffer from poorer stability [3, 4, 16, 17], even in alkaline conditions. It is unavoidable that catalyst materials will experience chemical or physical changes and eventual degradation when subjected to the harsh oxidative conditions of OER electrocatalysis. However, there are several methods available to mitigate the overall impact of this process. One intriguing approach to address stability concerns is the development of a catalyst that undergoes an *in-situ* chemical change resulting in improved catalytic activity.[2, 18-20] These materials are often referred to as pre-catalysts, as their initial state reacts under operating conditions to reach a more effective catalytic state. Given the highly oxidative conditions of OER catalysis, it is widely observed that chalcogens in the catalyst surface structure are replaced with oxygen to form oxide/hydroxide as more active sites,[21] but the continuous restructuring process from surface to bulk during the further cycling degrades the catalytic performance.[22-24] The initial restructuring leads to the formation of nanocluster moieties with more available active sites, and further restructuring leads to particle aggregation with less available active sites.[22-24] Consequently, the fully developed catalyst is thought to include the *in-situ* formation of this oxide surface component, while the bulk material retains its original structure. For example, our recent work on Co_9S_8 thin film electrocatalysts has demonstrated such surface composition and structural changes during OER.[2] Hence,

regulating the transition-metal sulfide structure during the reaction is vital for improving both catalytic activity and stability.[23, 25] Among different regulation strategies, doping is an effective way to populate novel active sites by introducing one or more active transition metals.[23, 25] Xie et al. have demonstrated Co doped NiS_2 exhibits a higher catalytic activity and stability than pure NiS_2.[26] Besides the single element doping, recent studies also investigate the dual-elements doping and multiple-elements doping (called high-entropy metal sulfide). Those studies all demonstrated excellent OER catalytic performance.[27, 28] However, the underlying restructuring processes and the role of metal doping in regulation are rarely studied, which hampers the development of restructured electrocatalysts.

Herein, we investigate a composition-regulated strategy for studying how doping mediates the restructuring progress. Specifically, we examine nickel cobalt sulfide catalyst nanoparticles embedded in carbon nanofibers ($Co_xNi_{1-x}S_y$). Through comprehensive analysis using X-ray photoelectron spectroscopy (XPS), X-ray absorption spectroscopy (XAS) analysis, and electrochemical measurements, we demonstrate that exposure to OER conditions induces a restructuring of the nickel and cobalt sulfide materials, which results in the formation of surface Co and Ni oxides/hydroxides nanoclusters with an edge-sharing octahedral local structure at the atomic scale, exhibiting favorable electrocatalytic activity for water oxidation. Moreover, we find that the catalytic performance can be influenced by adjusting the ratio between Ni and Co metals, allowing precise tuning of the electrocatalytic activity. Also, the Ni substitution, regulating the electron distribution around Ni and Co, leads to a different degree of restructuring, which affects the stability. Our experimental results suggest the role of Ni and Co in the restructuring processes which offers potential interests for future design of in-situ formed electrocatalyst.

2. Results and discussion

2.1. Characterizations of the as-synthesized materials

$Co_xNi_{1-x}S_y$ samples were prepared by electrospinning a precursor solution (Figure S1a), with detailed procedures outlined in the methods section. The Co and Ni ratio was chosen as pure Co_9S_8, $Co_{0.83}Ni_{0.17}$, $Co_{0.66}Ni_{0.33}$, $Co_{0.5}Ni_{0.5}$, $Co_{0.33}Ni_{0.67}$, $Co_{0.17}Ni_{0.83}$, and pure Ni_3S_2. Figure S2a illustrates powder X-ray diffraction (XRD) patterns for a series of samples with multiple compositional ratios of Ni to Co, with peaks corresponding to coexisting Co_9S_8 (COD No. 1011206) and Ni_3S_2 (COD No. 1011250) crystal structures. With more Ni substitution, the XRD peak around 32º becomes more pronounced while the XRD peak around 29º peak becomes weaker, which the Ni substitution would introduce some crystal structure change from Co_9S_8 to Ni_3S_2. The crystal structure is a bulk property that usually does not directly affect the catalytic

performance, but it may lead to different restructuring pathways. The coexistence of Co and Ni sulfur compounds is further confirmed by XPS analysis. Figures S3-S7 show XPS spectra of Ni 2p and Co 2p with peaks at 856 eV and 784 eV respectively, which have been ascribed to Ni and Co sulfides and sulfates. [25, 26] It is expected that metal sulfates present on the particle surface may contain a small degree of surface oxidation due to exposure to the atmosphere.

Scanning electron microscopy (SEM, Figure 1) shows the morphology and microstructure of the catalyst nanoparticles and their supporting carbon nanofibers, suggesting a good particle dispersion among an interconnected network of nanofibers. The energy dispersive spectroscopy confirms that all key elements are uniformly dispersed (Figure 1&S1), and the estimated element ratio of Co and Ni (Table S1) is close to the expected values. This evidence confirmed the successful synthesis of $Co_xNi_{1-x}S_y$.

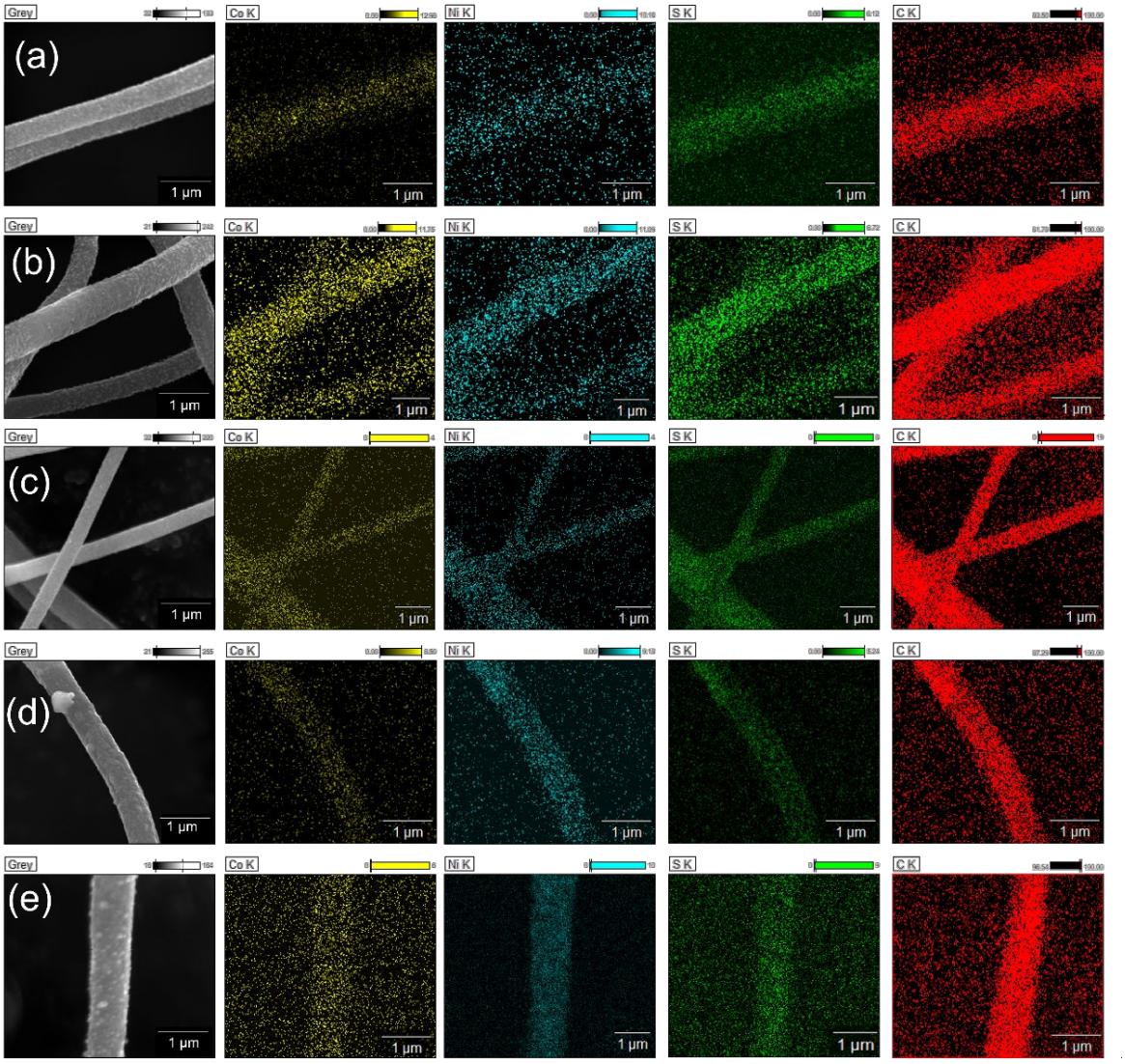

Figure 1. Microstructure and element mapping for (a) $Co_{0.83}Ni_{0.17}$; (b) $Co_{0.66}Ni_{0.33}$; (c) $Co_{0.5}Ni_{0.5}$; (d) $Co_{0.33}Ni_{0.67}$;(e) $Co_{0.17}Ni_{0.83}$; The Co, Ni, S, C elements are colored in yellow, blue, green, and red, respectively. (Co_9S_8 and Ni_3S_2 in Figure S1)

2.2. Electrochemical Measurements

$Co_xNi_{1-x}S_y$ samples were measured using a conventional three-electrode system immersed in 0.1 M KOH electrolyte. More experimental details can be found in the methods section. All current density measurements are normalized to geometric surface area.[29]

Figure 2a-2b show a comparison of the over-potentials obtained through cyclic voltammetry (CV) measurements for each prepared material and the standard RuO_2 at the first cycle. It demonstrates that the $Co_{0.83}Ni_{0.17}$ has the lowest over-potential at 5 mA cm^{-2} among all samples and is better than that of the standard RuO_2 (Figure 2d). Compared with the pure Co_9S_8 and Ni_3S_2, a small amount of Ni or Co substitution improves the OER performance. However, the OER performance gets worse when the Ni and Co ratio gets close to 1:1. The improved activity is also supported by the Tafel slope comparison in Figure 2c. Tafel slopes also indicate that Ni_3S_2 has a different reaction mechanism from that of Co_9S_8, and a small Ni substitution would not change the reaction mechanism such as $Co_{0.83}Ni_{0.17}$ and $Co_{0.67}Ni_{0.33}$ have almost the same Tafel slopes as that of Co_9S_8 (Figure 2d and Table S2). In addition, the CV data at the first cycle shows asymmetric oxidative and reductive peaks (Figure 2a and 2b). For example, $Co_{0.83}Ni_{0.17}$ has two oxidation peaks but only one reduction peak, and the oxidation peak area is much greater than the reduction peak area suggesting irreversible changes for all these materials. Drawing upon previous studies on sulfide electrocatalysts in OER [2, 15], these observed changes can be attributed to an irreversible restructuring process that transforms the pre-catalysts (Co_xNi_{1-x}) into more active phases, thereby enhancing the OER performance of the materials. By carefully integrating the peaks in the CV curve, it roughly shows that the $Co_{0.83}Ni_{0.17}$ composition exhibits the most pronounced oxidation peak, indicating the occurrence of substantial restructuring processes. Referring to previous studies on Co and Ni redox behaviors, two peaks for Co_9S_8 could be assigned to the Co^{2+}/Co^{3+} (peak around 1.2 V vs RHE) and Co^{3+}/Co^{4+} redox pairs (peak around 1.35 V vs RHE).[20, 30] Also, one peak for Ni_3S_2 could be assigned to the Ni^{3+}/Ni^{4+} redox pair (peak around 1.45 V vs RHE).[31, 32] Interestingly, the $Co_{0.83}Ni_{0.17}$ also displays two distinct oxidative peaks, which have the same first Co redox as Co_9S_8 but the later peak (around 1.4 V vs RHE) would be the mixture redox of Co and Ni during restructuring. [20, 31, 32] In contrast, the other $Co_xNi_{1-x}S_y$ catalysts exhibit only one oxidative peak, which could be mainly attributed to the mixture of Co and Ni redox process. The irreversible structure change led to activity loss for high Co contents ($x > 0.83$) and activity gain for relatively low Co contents ($x < 0.83$) except $Co_{0.17}Ni_{0.83}$ (Figure S2b). A careful investigation of the cycling data indicates that most materials undergo irreversible restructuring just after 1st cycle and almost reversible structuring in the following cycles (Figure

S2b-h) except $Co_{0.17}Ni_{0.83}$. The nearly reversible restructuring after 1st cycle imparts negligible change of catalytic performance, but the ongoing reversible structure change of $Co_{0.17}Ni_{0.83}$ results in performance decrease and then increase. In addition, the entirely different Tafel Slope in the 1st and 20th cycles (Table S2) indicates that the $Co_{0.17}Ni_{0.83}$ is still under irreversible structure change. Considering the restructured structure as the true active for the later cycles, pure NiO/NiOOH has better performance than CoO/CoOOH.[33, 34] That might be one reason why Ni_3S_2 has better catalytic performance than Co_9S_8 after serval cycles. However, the OER performance of bimetallic sulfides does not suggest that a high Ni ratio would necessarily lead to high performance since $Co_{0.67}Ni_{0.33}$ has better performance than $Co_{0.5}Ni_{0.5}$ after 20 cycles. This may be caused by different restructuring pathways and newly formed transition metal-oxygen bonding hybridization. In general, different Ni and Co ratios could regulate the restructuring processes of this bimetallic sulfide, which we would like to further investigate by XPS and in situ XAS.

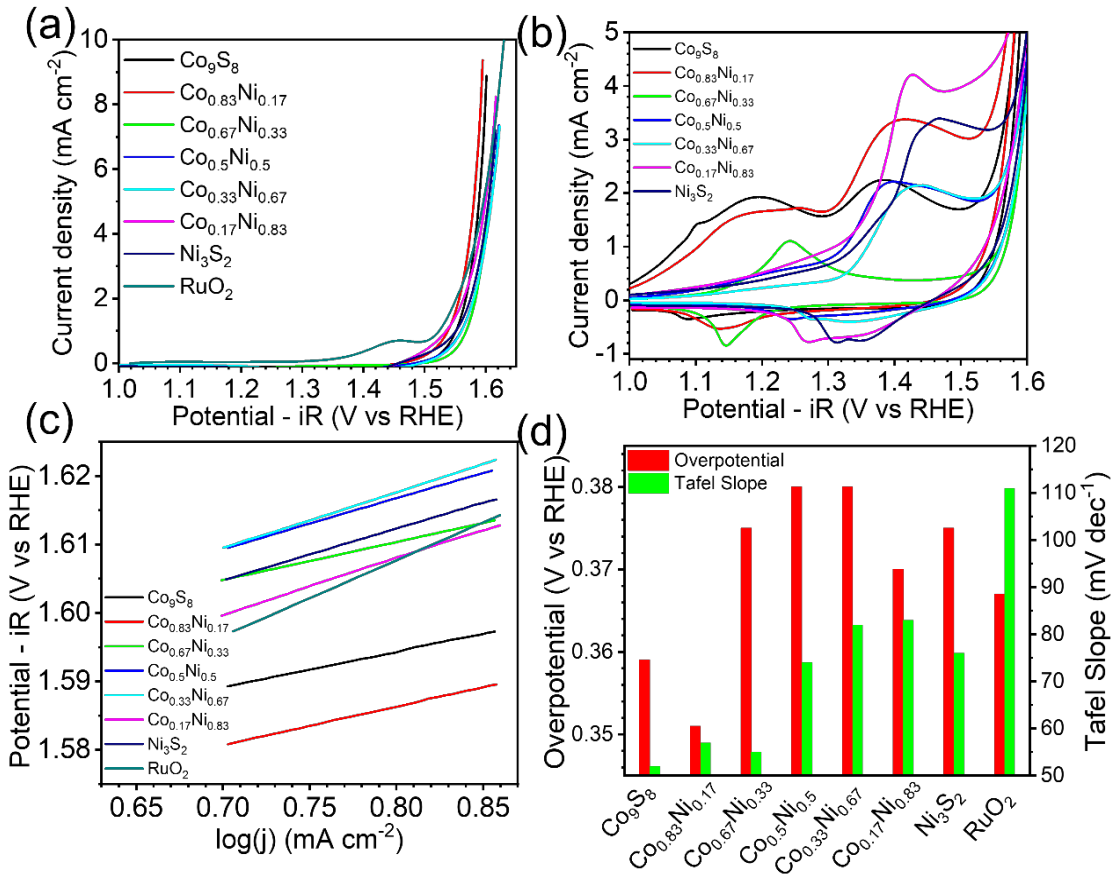

Figure 2. Electrochemical results from cyclic voltammetry, (a) OER performance of $Co_xNi_{1-x}S_y$ materials and RuO_2 at the first cycle (b) Enlarged CV data of figure a (c) Tafel slope of $Co_xNi_{1-x}S_y$ materials and RuO_2 (d) the over-potential values of $Co_xNi_{1-x}S_y$ materials at 5 mA cm^{-2} and the Tafel Slope values extracted from figure 2c.

2.3. Mechanistic Understanding

To clearly understand how Ni and Co doping regulate the restructuring and its relationship with electrochemical performance, ex-situ XPS was carried out to analyze the surface chemical composition and chemical binding. Chemical composition is one crucial parameter to help understand the changing electrocatalytic performance between different metal compositions. Figure 3 compares the XPS spectra of Co_9S_8 and Ni_3S_2 materials before and after cycling under OER conditions. There is a clear reduction in peak area in the S 2p 164 eV region as shown in Figure 3a&d, which corresponds to metal sulfides.[35, 36] It is worth noting that even in pristine samples, the surface already contains surface-adsorbed oxygen/metal hydroxides as the active sites (Figure 3b&c, Figure S3-S7), but the majority of the bulk is still metal sulfide.[37-39] The detailed fitting of O 2p XPS (Table 1&S5) indicates that the sample with higher Ni contents (when X<0.83) would have more surface adsorbed oxygen/hydroxides after cycling, which generates more active sites. That is one possible reason for the increased catalytic performance. Oppositely, both Co_9S_8 and $Co_{0.83}Ni_{0.17}$ show a lower amount of surface oxygen/hydroxide after the reaction, which corresponds to lower active sites. Besides those surface oxygen/hydroxide, there is one new peak around 530eV in cycled Co_9S_8 and $Co_{0.83}Ni_{0.17}$ responsible for the bulk metal oxide bond.[37-39] The bulk metal oxide formation would be another reason for the inferior stability. [40, 41]

Additionally, we observe an increase in Co^{3+} at 781 eV and an accompanying decrease in Co^{2+} at 784 eV in the Co2p spectra (Figure 3c), and a significant increase in nickel components both as Ni^{3+} and Ni^{2+} at 862 eV and 856 eV, respectively, in the Ni 2p spectra (Figure 3f) after exposure to OER conditions.[40, 42] Those correspond to the oxidation states of both Co and Ni due to surface oxygen/hydroxide under harsh OER conditions.[43-45] However, the detailed peaking fitting results suggest an overall reduced oxidation state of Ni and increased oxidation of Co (Table S3 & S4). The same behavior happens for all $Co_xNi_{1-x}S_y$ samples (Figure S3-7 and Table S3&4). All XPS data of cycled materials show higher intensity of Co^{3+}, Co^{2+}, Ni^{3+}, and Ni^{2+}, but reduced Ni oxidation state and increased Co oxidation state. Co may be more easily oxidized to form bulk particles than Ni. This is why the Ni substitution can reduce the surface restructuring to control the stability. However, all $Co_xNi_{1-x}S_y$ contain low oxidation states of Co and Ni (lower than 2), which is hard to distinguish from XPS. Hence, Co and Ni K-edge X-ray absorption spectroscopy (XAS) were carried out to evaluate the electronic and atomic structure change.[46-49]

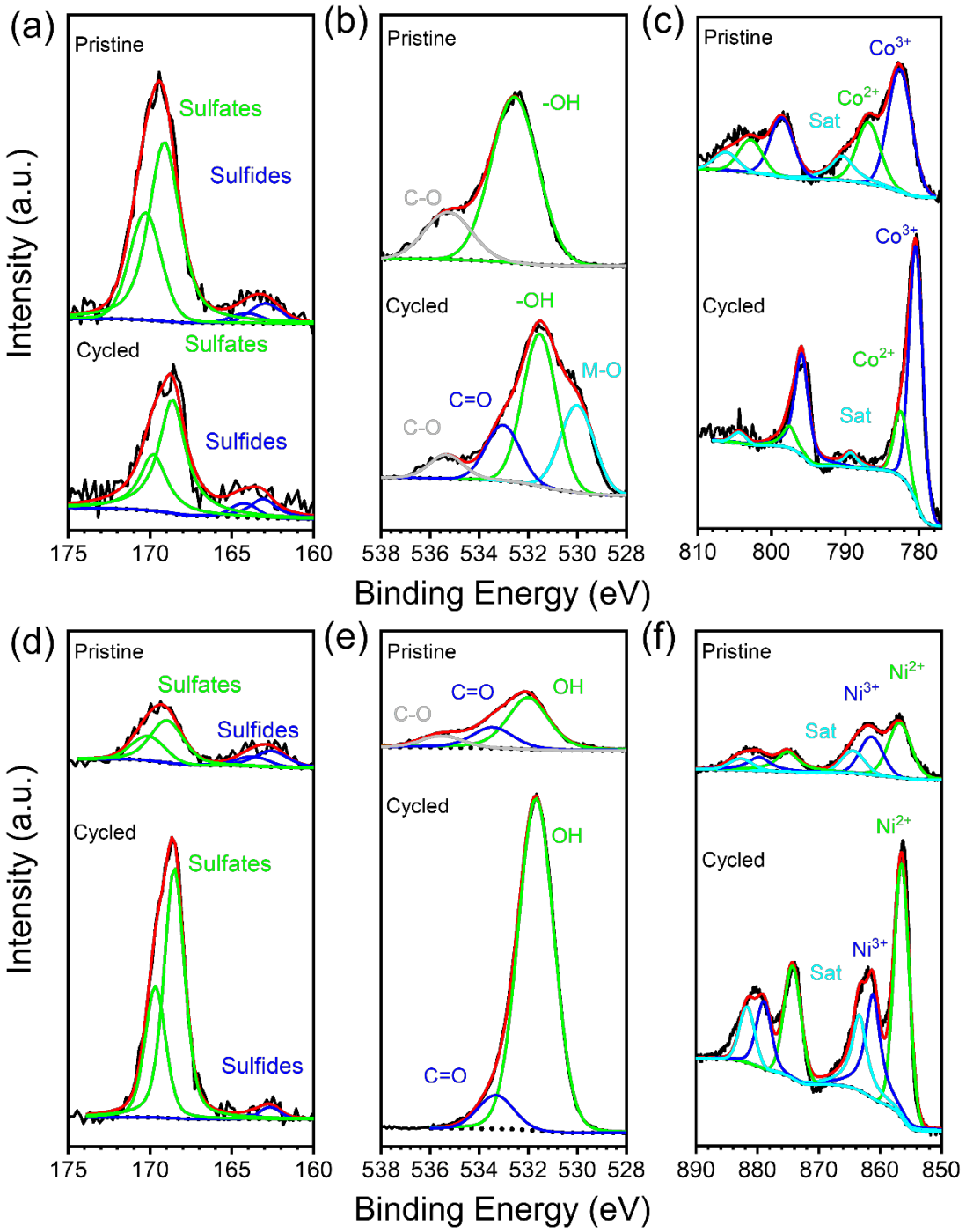

Figure 3. XPS of Co_9S_8 material as synthesized (Pristine) and after OER (Cycled), (a) S 2p, (b) O 1s, (c) Co 2p; XPS of Ni_3S_2 material as synthesized (Pristine) and after OER (Cycled), (a) S 2p, (b) O 1s, (c) Ni 2p

Table 1: Co and Ni oxidation state of $Co_xNi_{1-x}S_y$ materials from XANES; OH and M-O percent of $Co_xNi_{1-x}S_y$ materials from XPS; $Co_xNi_{1-x}S_y$ restructuring percentage after 20 cycles from XANES; Overpotential of $Co_xNi_{1-x}S_y$ materials at 5mA cm^{-2}

	Co		Ni		OH (%)		M-O (%)		Restructuring (%)		Overpotential(mV)	
	pri	20th	pri	20th	pri	20th	pri	20th	Co:20th	Ni: 20th	1st	20th
Co_9S_8	0.80	2.31	/	/	0.78	0.47	0.00	0.27	84.5	/	0.359	0.384
$Co_{0.83}Ni_{0.17}$	0.92	2.43	1.91	2.20	0.70	0.66	0	0.13	94.3	65.5	0.351	0.368
$Co_{0.63}Ni_{0.37}$	0.90	1.26	1.73	1.40	0.55	0.74	0	0	28.3	18.9	0.375	0.360
$Co_{0.5}Ni_{0.5}$	0.52	1.34	1.35	1.41	0.77	0.84	0	0	31.0	22.8	0.380	0.371
$Co_{0.37}Ni_{0.63}$	0.60	1.41	1.31	1.46	0.48	0.76	0	0	35.4	24.6	0.380	0.357
$Co_{0.17}Ni_{0.83}$	1.18	1.83	1.00	1.81	0.40	0.79	0	0	57.8	46.5	0.370	0.406
Ni_3S_2	/	/	1.04	2.00	0.62	0.91	0	0	/	60.9	0.375	0.341

Co K-edge X-ray absorption near edge structure (XANES) indicates the Co was oxidized during the OER reaction (Figure 4a). The Co_9S_8, $Co_{0.83}Ni_{0.17}$, and $Co_{0.17}Ni_{0.83}$ show obvious shifts in the Co edge positions, which indicates clear oxidation of Co, but the other samples only display minor differences between the pristine material and the cycled material. Ni in the $Co_{0.83}Ni_{0.17}$, $Co_{0.17}Ni_{0.83}$, and Ni_3S_2, shows a similar trend to Co (Figure 4b), undergoing significant oxidation after cycling, but the remaining samples do not show any apparent change in Ni oxidation. To quantify the amount of Co and Ni oxidized during OER, linear combination fitting of XANES was carried out (Figure 4c and Table 1&S6-S7) by using corresponding pristine, Co standards, and Ni standards.[50, 51] The fitting analysis illustrates that the largest conversion of both Co and Ni took place in the $Co_{0.83}Ni_{0.17}$ sample, with more than 90% of the original catalysts being converted to oxides. The high percentage conversion of the original pre-catalysts to oxides also suggests that not only the materials' surface but also some core bulk materials undergo restructuring. The large amount of restructured nanocluster would aggregate together to become bulky metal oxide particles to deactivate the catalysts. Ni_3S_2 has a relatively low amount of conversion compared with Co_9S_8 and $Co_{0.83}Ni_{0.17}$, which consists of the O 1s XPS results. Further detailed calculation of oxidation by using a linear relationship between XANES edge position and oxidation state (Table 1&S8) also confirmed that Co_9S_8, $Co_{0.83}Ni_{0.17}$, $Co_{0.17}Ni_{0.83}$, and Ni_3S_2 undergo obvious oxidation state changes. In addition, all those Co and Ni ions in $Co_xNi_{1-x}S_y$ demonstrate a lower Co and Ni oxidation state than the regular valence of 2+, which also helps explain the observed increased intensity of Co(II&III) and Ni(II&III) in

XPS results. More interestingly, the comparison between different $Co_xNi_{1-x}S_y$ materials with standard Co_9S_8 and Ni_3S_2 (Figure S9a&b) illustrates that Ni substitution could change the electron distribution around Co. Based on XRD results (Figure S2), $Co_{0.83}Ni_{0.17}$ and $Co_{0.17}Ni_{0.83}$ have the very similar crystal structure as Co_9S_8 and Ni_3S_2, respectively, whereas $Co_{0.67}Ni_{0.33}$ $Co_{0.5}Ni_{0.5}$, and $Co_{0.33}Ni_{0.67}$ form a new phase or mixed phase. The Ni and Co would balance the electron distribution in the new/mixed phase to keep at a lower oxidation state to improve stability (Table 1&S8). In addition, a small amount of Ni substitution ($Co_{0.83}Ni_{0.17}$) induced high valence Ni which improves the starting catalytic activity but is not able to improve the stability. Also, a small amount of Co substitution ($Co_{0.17}Ni_{0.83}$) does not contribute to the catalytic activity, but the high amount of Co (Co_9S_8 and $Co_{0.83}Ni_{0.17}$) restructures a lot (high Co oxidation state) after 20 cycles block the active sites.

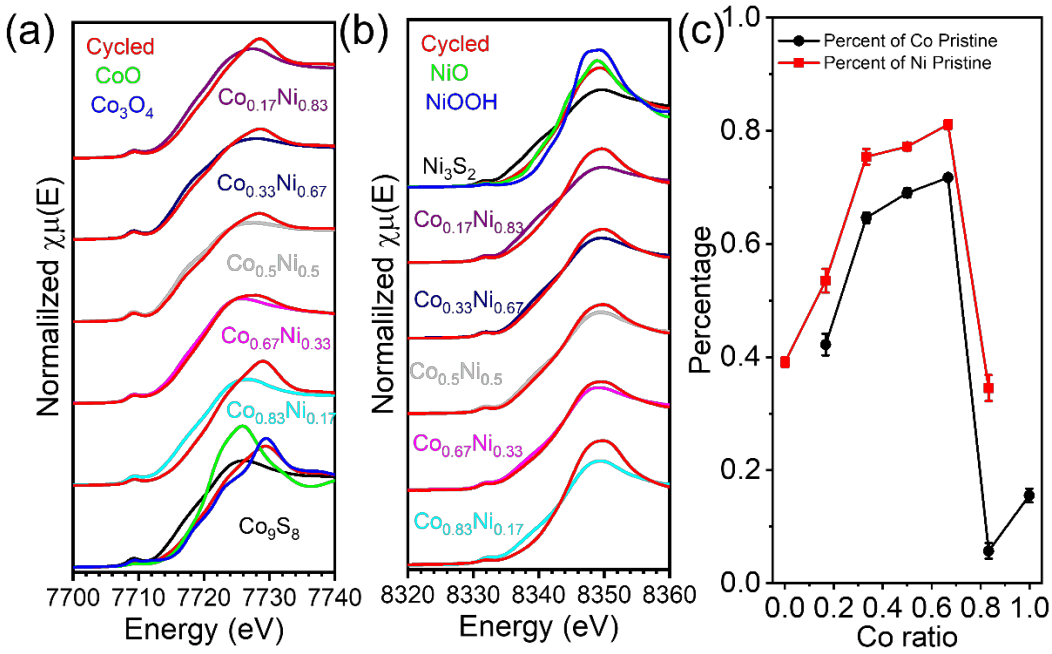

Figure 4. (a) Co K-edge XANES (the red line is the corresponding samples after the OER reaction, the green line is standard CoO, the blue line is standard Co_3O_4); (b) Ni K-edge XANES (the red line is the corresponding samples after the OER cycles, the green line is standard NiO, the blue line is standard NiOOH); (c) Linear Combination fitting of Co K-edge XANES and Ni K-edge XANES.

A similar trend was also found in the extended X-ray absorption fine structure (EXAFS). Figure 5b shows the Co K-edge EXAFS, wherein a notable shift in the first peak position was observed, changing from 1.8 Å to 1.5 Å in Co_9S_8, $Co_{0.83}Ni_{0.17}$, and $Co_{0.17}Ni_{0.83}$. This shift signifies a transition from Co-S bonding to Co-O bonding. Also, a sharp second peak at 2.4 Å emerged, which stands for the new Co-O-Co/Ni bonding formation. Similarly, figure 5c demonstrates a shift in the first peak position from 1.9 Å to 1.6 Å in both $Co_{0.83}Ni_{0.17}$ and Ni_3S_2, denoting a

shift from Ni-S bonding to Ni-O bonding. The sharp second peak at 2.4 Å indicating Ni-O-Ni/Co bonding is also evident. The EXAFS results agree well with XANES and XPS results. The newly formed metal-oxygen bonding and metal-oxygen-metal bonding signifies the formation of metal oxides/hydroxides nanoclusters, which likely serve as the actual active catalytic phase. Furthermore, the lower intensity of the newly formed peak (around 2.4 Å) indicates that $Co_{0.67}Ni_{0.33}$ $Co_{0.5}Ni_{0.5}$, and $Co_{0.33}Ni_{0.67}$ does not undergo significant restructuring (Figure 5b&c) to form bulk metal oxide. This phenomenon also agrees with XANES and XPS results that Ni substitution could regulate the restructuring rate.

To determine the precise structure of the newly formed nanoclusters on the surfaces, we conducted an EXAFS model-based analysis for the standard Co_9S_8 and Ni_3S_2 (Figure 5a).[2, 50, 51] The EXAFS fitting results (Figure S10-S12, table S9-S10) indicate the formation of Co-O, Ni-O, and Co/Ni-O-Co/Ni bonding, which does not exist in the pristine materials. The bonding lengths for Co-O, Ni-O, and Co/Ni-O-Co/Ni (Table S9-S10) suggest the formation of edge-sharing octahedra structures based on the previous literature.[52, 53] Our recent *in-situ* XAS work on Co_9S_8 film restructuring processes supported the notion that the edge-sharing octahedra units are the true active sites for the OER.[2] Since the true active sites are in-situ reaction generated, the size of the cluster and the newly formed transition-metal-oxygen hybridization bond are both critical to the catalytic activity,[54, 55] and the restructuring rate is more critical to both activity and stability. Hence, we posit that both the newly formed bonding and the degree of restructuring collectively impact the OER performance.

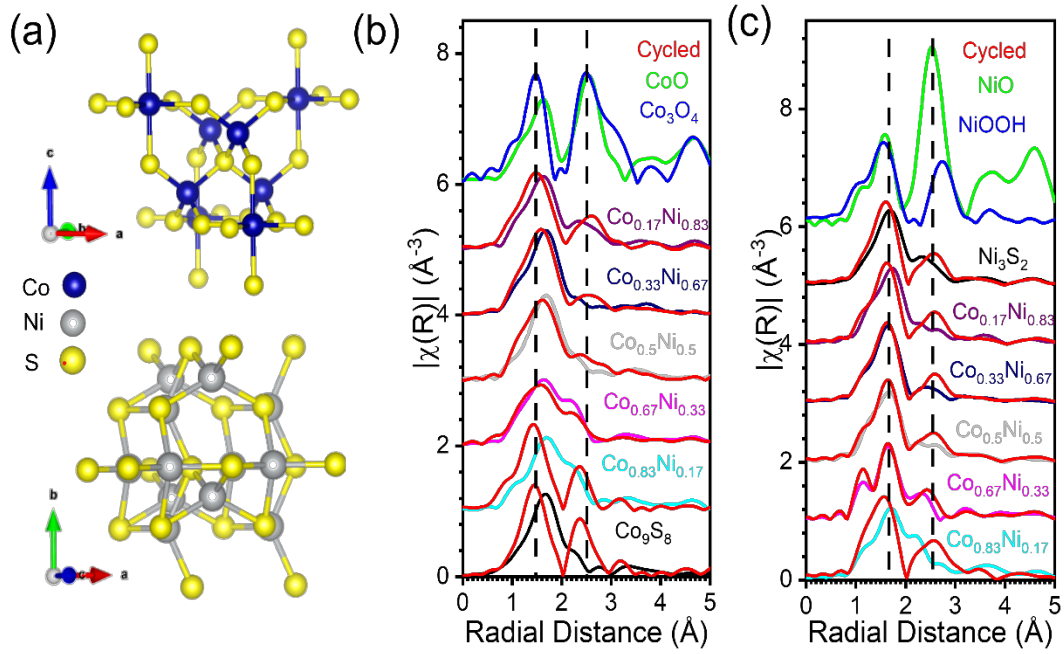

Figure 5. (a) Schematic of Co_9S_8 and Ni_3S_2 crystal structure used in EXAFS fitting; (b) Co K-edge Fourier Transformed R-space of $Co_xNi_{1-x}S_y$, (the red line is the corresponding samples

after the OER reaction, the green line is standard CoO, the blue line is standard Co_3O_4); (c) Ni K-edge Fourier Transformed R-space of $Co_xNi_{1-x}S_y$, (the red line is the corresponding samples after the OER cycles, the green line is standard NiO, the blue line is standard NiOOH)

3. Conclusion

In summary, we successfully regulate the $Co_xNi_{1-x}S_y$ restructuring processes by adjusting the Co and Ni compositional ratio. Electrochemical analysis revealed that small Ni substitution (X = 0.17) would generally enhance the OER activity and more Ni substitution ($0.17 < X < 0.83$) would reduce the restructuring rate to enhance the stability. To gain insights into the underlying relationship around local structure, restructuring, and electrocatalytic performance, we performed XPS and XAS measurements and analysis. Our XPS results indicated that OER exposure leads to surface oxidation, particularly forming metal hydroxides/surface adsorbed oxygen. This in-situ transformation to an oxygen-rich surface facilitated parallel pathways to water oxidation, thereby enhancing OER performance, especially for the $Co_{0.83}Ni_{0.17}$ regulated composition. However, the high Co content (Co_9S_8 and $Co_{0.83}Ni_{0.17}$) would quickly restructure into bulk metal oxide formation and lose some available active sites. The Ni substitution would inhibit this bulk metal oxide formation. XAS analysis through XANES and EXAFS supported our XPS findings, providing evidence for a synergistic effect between Ni and Co: small Ni substitution improves activity but not stability and a higher amount of Ni substitution improves stability but not activity. Furthermore, we confirmed that metal sulfide converts to the more active phase, which is believed to involve metal oxide/hydroxide nanoclusters. The metal-oxygen-hybridization and size of the cluster further determine the catalytic activity, and the speed of bulk metal oxide formation affects the stability. Our work demonstrates that the strategic tuning of electrocatalytic properties through the mixed usage of Ni and Co, combined with the transformative effect of harshly oxidative OER conditions on catalyst materials, represents a new strategy. The utilization of *in-situ* restructuring from a pre-catalyst should be further explored and applied more broadly, as it holds significant promise for advancing the field of OER electrocatalysis in the near future.

Supporting Information

Supporting Information is available from the Wiley Online Library or from the author.

Acknowledgements

This work is supported by the National Science Foundation under No. CBET-2016192, CBET-1949870, and DMR-1832803. Part of this research was conducted at the Northwest Nanotechnology Infrastructure, a National Nanotechnology Coordinated Infrastructure site at Oregon State University which is supported in part by the National Science Foundation (grant

NNCI-2025489) and Oregon State University. The use of 9-BM of APS of Argonne National Laboratory (ANL) for synchrotron XAS measurements is supported by Department of Energy Office of Basic Energy Sciences, and the use of XPS at Post Test Facility of ANL is supported by Department of Energy, Office of Energy Efficiency and Renewable Energy (EERE), under Contract No. DE-AC02-06CH11357.

Received: ((will be filled in by the editorial staff))
Revised: ((will be filled in by the editorial staff))
Published online: ((will be filled in by the editorial staff))

References

[1] C. Cai; M. Y. Wang; S. B. Han; Q. Wang; Q. Zhang; Y. M. Zhu; X. M. Yang; D. J. Wu; X. T. Zu; G. E. Sterbinsky; Z. X. Feng; M. Gu, *ACS Catalysis* **2021,** *11* (1), 123-130.
[2] M. Wang; Q. Wa; X. Bai; Z. He; W. S. Samarakoon; Q. Ma; Y. Du; Y. Chen; H. Zhou; Y. Liu; X. Wang; Z. Feng, *JACS Au* **2021,** *1* (12), 2216-2223. DOI 10.1021/jacsau.1c00346.
[3] Y. T. Yan; P. C. Wang; J. H. Lin; J. Cao; J. L. Qi, *Journal of Energy Chemistry* **2021,** *58*, 446-462. DOI 10.1016/j.jechem.2020.10.0102095-4956/.
[4] G. A. Gebreslase; M. V. Martinez-Huerta; M. J. Lazaro, *Journal of Energy Chemistry* **2022,** *67*, 101-137. DOI 10.1016/j.jechem.2021.10.009.
[5] J. F. Qin; J. H. Lin; T. S. Chen; D. P. Liu; J. Y. Xie; B. Y. Guo; L. Wang; Y. M. Chai; B. Dong, *Journal of Energy Chemistry* **2019,** *39*, 182-187. DOI 10.1016/j.jechem.2019.01.022.
[6] Y. J. Li; W. Y. Wang; B. J. Huang; Z. F. Mao; R. Wang; B. B. He; Y. S. Gong; H. W. Wang, *Journal of Energy Chemistry* **2021,** *57*, 99-108. DOI 10.1016/j.jechem.2020.08.064.
[7] D. X. Yang; W. Q. Hou; Y. J. Lu; W. L. Zhang; Y. F. Chen, *Journal of Energy Chemistry* **2021,** *52*, 130-138. DOI 10.1016/j.jechem.2020.04.005.
[8] T. Y. Wang; C. Wang; Y. Jin; A. Sviripa; J. S. Liang; J. T. Han; Y. H. Huang; Q. Li; G. Wu, *J Mater Chem A* **2017,** *5* (48), 25378-25384. DOI 10.1039/c7ta08720a.
[9] K. Wan; J. S. Luo; X. Zhang; P. Subramanian; J. Fransaer, *Journal of Energy Chemistry* **2021,** *62*, 198-203. DOI 10.1016/j.jechem.2021.03.013.
[10] L. Wang; W.-W. Tian; W. Zhang; F. Yu; Z.-Y. Yuan, *Applied Catalysis B: Environmental* **2023,** *338*, 123043. DOI https://doi.org/10.1016/j.apcatb.2023.123043.
[11] H.-Y. Wang; L. Wang; J.-T. Ren; W. Tian; M. Sun; Y. Feng; Z.-Y. Yuan, *Acs Nano* **2023,** *17* (11), 10965-10975. DOI 10.1021/acsnano.3c03095.
[12] U. Shamraiz; A. Badshah; B. Raza, *Langmuir* **2020,** *36* (9), 2223-2230.
[13] A. G. Rajan; J. M. P. Martirez; E. A. Carter, *Journal of the American Chemical Society* **2020,** *142* (7), 3600-3612.
[14] X. K. Wang; G. M. Zhan; Y. R. Wang; Y. Zhang; J. Zhou; R. Xu; H. Y. Gai; H. L. Wang; H. Q. Jiang; M. H. Huang, *Journal of Energy Chemistry* **2022,** *68*, 113-123. DOI 10.1016/j.jechem.2021.09.014.
[15] W. Zhang; L. Wang; L.-H. Zhang; D. Chen; Y. Zhang; D. Yang; N. Yan; F. Yu, *Chemsuschem* **2022,** *15* (12), e202200195. DOI https://doi.org/10.1002/cssc.202200195.

[16] F. Zeng; C. Mebrahtu; L. F. Liao; R. Palkovits; A. K. Beine, *Journal of Energy Chemistry* **2022,** *69*, 301-329. DOI 10.1016/j.jechem.2022.01.025.
[17] Z. K. Chen; X. K. Wang; S. Kessler; Q. Q. Fan; M. H. Huang; H. Colfen, *Journal of Energy Chemistry* **2022,** *71*, 89-97. DOI 10.1016/j.jechem.2022.02.0422095-4956.
[18] B. R. Wygant; K. Kawashima; C. B. Mullins, *ACS Energy Letters* **2018,** *3* (12), 2956-2966.
[19] G. Wan; J. W. Freeland; J. Kloppenburg; G. Petretto; J. N. Nelson; D. Y. Kuo; C. J. Sun; J. G. Wen; J. T. Diulus; G. S. Herman; Y. Q. Dong; R. H. Kou; J. Y. Sun; S. Chen; K. M. Shen; D. G. Schlom; G. M. Rignanese; G. Hautier; D. D. Fong; Z. X. Feng; H. Zhou; J. Suntivich, *Science Advances* **2021,** *7* (2), eabc7323.
[20] Y. Chen; Y. Sun; M. Wang; J. Wang; H. Li; S. Xi; C. Wei; P. Xi; E. Sterbinsky George; W. Freeland John; C. Fisher Adrian; W. Ager Joel; Z. Feng; J. Xu Zhichuan, *Science Advances* **2021,** *7* (50), eabk1788. DOI 10.1126/sciadv.abk1788.
[21] W. Adamson; C. Jia; Y. Li; C. Zhao, *Electrochim Acta* **2020,** *355*, 136802. DOI https://doi.org/10.1016/j.electacta.2020.136802.
[22] H. N. Jia; N. Yao; J. Zhu; W. Luo, *Chem-Eur J* **2023,** *29* (13). DOI ARTN e202381362
10.1002/chem.202381362.
[23] R. Z. He; X. Y. Huang; L. G. Feng, *Energ Fuel* **2022,** *36* (13), 6675-6694. DOI 10.1021/acs.energyfuels.2c01429.
[24] J.-T. Ren; L. Chen; W.-W. Tian; X.-L. Song; Q.-H. Kong; H.-Y. Wang; Z.-Y. Yuan, *Small* **2023,** *19* (27), 2300194. DOI https://doi.org/10.1002/smll.202300194.
[25] Y. H. Wang; N. N. Chen; X. Q. Du; X. H. Han; X. S. Zhang, *J Alloy Compd* **2022,** *893*. DOI ARTN 162269
10.1016/j.jallcom.2021.162269.
[26] S. L. Xie; J. X. Gou; B. Liu; C. G. Liu, *Inorganic Chemistry Frontiers* **2018,** *5* (5), 1218-1225. DOI 10.1039/c8qi00172c.
[27] M. J. Cui; C. P. Yang; B. Y. Li; Q. Dong; M. L. Wu; S. Hwang; H. Xie; X. Z. Wang; G. F. Wang; L. B. Hu, *Adv Energy Mater* **2021,** *11* (3). DOI ARTN 2002887
10.1002/aenm.202002887.
[28] Y. R. Hong; S. Mhin; K. M. Kim; W. S. Han; H. Choi; G. Ali; K. Y. Chung; H. J. Lee; S. I. Moon; S. Dutta; S. Sun; Y. G. Jung; T. Song; H. Han, *J Mater Chem A* **2019,** *7* (8), 3592-3602. DOI 10.1039/c8ta10142f.
[29] W. Chen; Y. Y. Liu; Y. Z. Li; J. Sun; Y. C. Qiu; C. Liu; G. M. Zhou; Y. Cui, *Nano Lett* **2016,** *16* (12), 7588-7596.
[30] A. Moysiadou; S. Lee; C.-S. Hsu; H. M. Chen; X. Hu, *Journal of the American Chemical Society* **2020,** *142* (27), 11901-11914. DOI 10.1021/jacs.0c04867.
[31] C. Kuai; Y. Zhang; L. Han; H. L. Xin; C.-J. Sun; D. Nordlund; S. Qiao; X.-W. Du; F. Lin, *J Mater Chem A* **2020,** *8* (21), 10747-10754. DOI 10.1039/D0TA04244G.
[32] N. Zhang; X. Feng; D. Rao; X. Deng; L. Cai; B. Qiu; R. Long; Y. Xiong; Y. Lu; Y. Chai, *Nat Commun* **2020,** *11* (1), 4066. DOI 10.1038/s41467-020-17934-7.
[33] N. Ullah; W. Zhao; X. Lu; C. J. Oluigbo; S. A. Shah; M. Zhang; J. Xie; Y. Xu, *Electrochim Acta* **2019,** *298*, 163-171. DOI https://doi.org/10.1016/j.electacta.2018.12.053.
[34] B. J. Taitt; D. H. Nam; K. S. Choi, *Acs Catal* **2019,** *9* (1), 660-670. DOI 10.1021/acscatal.8b04003.
[35] J. Zhang; T. Wang; D. Pohl; B. Rellinghaus; R. Dong; S. Liu; X. Zhuang; X. Feng, *Angewandte Chemie International Edition* **2016,** *55* (23), 6702-6707. DOI https://doi.org/10.1002/anie.201602237.
[36] L.-L. Wu; Q.-S. Wang; J. Li; Y. Long; Y. Liu; S.-Y. Song; H.-J. Zhang, *Small* **2018,** *14* (20), 1704035. DOI https://doi.org/10.1002/smll.201704035.

[37] B. C. Qiu; L. J. Cai; Y. Wang; X. Y. Guo; S. N. Ma; Y. Zhu; Y. H. Tsang; Z. J. Zheng; R. K. Zheng; Y. Chai, *Small* **2019,** *15* (45). DOI ARTN 1904507 10.1002/smll.201904507.
[38] H. X. Zhang; J. Y. Wang; Q. L. Cheng; P. Saha; H. Jiang, *Green Energy Environ* **2020,** *5* (4), 492-498. DOI 10.1016/j.gee.2020.07.010.
[39] T. C. Khiem; N. N. Huy; E. Kwon; X. G. Duan; S. Waclawek; J. Bedia; Y. C. Tsai; A. Ebrahimi; F. Ghanbari; K. Y. A. Lin, *Applied Catalysis B-Environment and Energy* **2023,** *330*. DOI ARTN 122550 10.1016/j.apcatb.2023.122550.
[40] J. Haber; J. Stoch; L. Ungier, *J Electron Spectrosc* **1976,** *9* (5), 459-467. DOI https://doi.org/10.1016/0368-2048(76)80064-3.
[41] T. Takahagi; I. Shimada; M. Fukuhara; K. Morita; A. Ishitani, *Journal of Polymer Science Part A: Polymer Chemistry* **1986,** *24* (11), 3101-3107. DOI https://doi.org/10.1002/pola.1986.080241134.
[42] Y. Qi; Z. Yang; S. Peng; M. Wang; J. Bai; H. Li; D. Xiong, *Inorganic Chemistry Frontiers* **2021,** *8* (18), 4247-4256. DOI 10.1039/D1QI00693B.
[43] L. F. Li; Y. F. Li; Z. P. Liu, *Acs Catalysis* **2020,** *10* (4), 2581-2590.
[44] D. Friebel; M. W. Louie; M. Bajdich; K. E. Sanwald; Y. Cai; A. M. Wise; M. J. Cheng; D. Sokaras; T. C. Weng; R. Alonso-Mori; R. C. Davis; J. R. Bargar; J. K. Norskov; A. Nilsson; A. T. Bell, *Journal of the American Chemical Society* **2015,** *137* (3), 1305-1313. DOI 10.1021/ja511559d.
[45] B. Kim; A. Oh; M. K. Kabiraz; Y. Hong; J. Joo; H. Baik; S. I. Choi; K. Lee, *Acs Applied Materials & Interfaces* **2018,** *10* (12), 10115-10122.
[46] M. Wang; Z. Feng, *Current Opinion in Electrochemistry* **2021**, 100803.
[47] A. Bergmann; T. E. Jones; E. M. Moreno; D. Teschner; P. Chernev; M. Gliech; T. Reier; H. Dau; P. Strasser, *Nat Catal* **2018,** *1* (9), 711-719. DOI 10.1038/s41929-018-0141-2.
[48] Y. Duan; S. N. Sun; S. B. Xi; X. Ren; Y. Zhou; G. L. Zhang; H. T. Yang; Y. H. Du; Z. C. J. Xu, *Chem Mater* **2017,** *29* (24), 10534-10541. DOI 10.1021/acs.chemmater.7b04534.
[49] E. Fabbri; R. Mohamed; P. Levecque; O. Conrad; R. Kotz; T. J. Schmidt, *Acs Catalysis* **2014,** *4*, 1061-1070. DOI 10.1021/cs400903k.
[50] M. Newville, *Rev Mineral Geochem* **2014,** *78*, 33-74. DOI 10.2138/rmg.2014.78.2.
[51] S. Calvin, *XAFS for Everyone*. CRC Press: Hoboken, **2013**.
[52] M. W. Kanan; J. Yano; Y. Surendranath; M. Dinca; V. K. Yachandra; D. G. Nocera, *Journal of the American Chemical Society* **2010,** *132* (39), 13692-13701. DOI 10.1021/ja1023767.
[53] A. Mansour; C. Melendres, *X-ray absorption spectra and structure of some nickel oxides (hydroxides)*. **1994**.
[54] J. Suntivich; K. J. May; H. A. Gasteiger; J. B. Goodenough; Y. Shao-Horn, *Science* **2011,** *334* (6061), 1383.
[55] W. L. Xu; W. D. Zhong; C. F. Yang; R. Zhao; J. Wu; X. K. Li; N. J. Yang, *Journal of Energy Chemistry* **2022,** *73*, 330-338. DOI 10.1016/j.jechem.2022.06.042.

ToC figure:

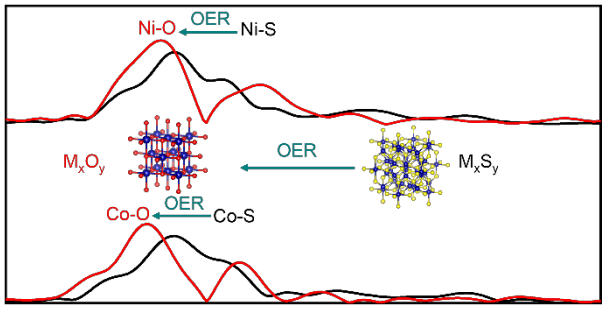

Restructuring plays a crucial role in electrocatalysts, influencing both catalytic activity and stability. Both Ni_3S_2 and Co_9S_8 restructure into nano-metal hydroxides, which enhance activity initially. However, continuous restructuring may result in the formation of large bulk metal hydroxides that lead to a loss of activity. Doping Ni or Co can modify the electronic structures, thereby regulating the restructuring processes. This offers a novel approach to balancing activity and stability in electrocatalysts.